Book of abstracts

2nd Population Balance Modeling Webinar

25th November 2024

2nd Population Balance Modeling Webinar
25th November 2024, online

Population Balance Modeling of emulsions preparation: Uncertainty and sensitivity analysis

Touma Kristy[1], Lebaz Noureddine[1] and Othman Nida[1]

[1]Universite Claude Bernard Lyon 1, CNRS, LAGEPP UMR 5007, F-69100, Villeurbanne, France
Corresponding author email: kristy.touma@univ-lyon1.fr

ABSTRACT

Emulsions are used in diverse industries such as food, cosmetics, and pharmaceuticals. The population balance equation is a suitable framework largely used for the modeling of emulsion preparation. Within this framework, phenomena such as droplet breakage and coalescence are modeled by phenomenological kernels. However, discrepancies in the governing parameters often arise due to scale or application differences. This research aims to determine the conditions of proper parameter identifiability as well as kernels selection, leading to a broadly applicable model.

Keywords: parameter identifiability, uncertainty, sensitivity, Markov Chain Monte Carlo simulation.

1. Introduction

1.1. Modeling approach

Emulsions are prepared using open-cell solid foams (OCSF) inserted inside a pipe, a method we have previously demonstrated to be both efficient and energy-competitive in continuous mode (Lebaz et al., 2024). This setup ensures a uniform energy dissipation, enabling us to apply the Population Balance Modeling (PBM) approach to model the dynamic evolution of the droplet size distribution without a need for CFD coupling.

Given the low dispersed phase fraction (1 %) in our study, we focused on the breakage mechanism, which can be modelled by two key functions: breakage probability *S* and daughter size distribution β (Equation 1). Numerous models exist for these functions, reflecting their complexity. We first compare two widely-used breakage kernels: Coulaloglou and Tavlarides (Equation 2) and Alopaeus et al. For the daughter size distribution, we used the Lee et al. model, assuming a uniform beta distribution with parameters a=b=2 (Equation 3). Breakage probability models include parameters B_1, B_2 and B_3, with research showing significant variability in their values across different studies and scales.

$$\frac{\partial n(t,x)}{\partial t} = \int_x^\infty b(t,x,x')S(t,x')n(t,x')dx' \; - S(t,x)n(t,x) \tag{1}$$

$$S(t,\varepsilon) = B_1 d_i^{-2/3}\varepsilon^{1/3}\exp\left[-B_2\frac{\sigma}{\rho_c^{\frac{2}{3}}\varepsilon^{\frac{2}{3}}d_i^{\frac{5}{3}}} - B_3\frac{\mu_d}{\sqrt{\rho_c\rho_d}\varepsilon^{1/3}d_i^{4/3}}\right] \tag{2}$$

$$\beta(t,x,\varepsilon) = \frac{\Gamma(a+b)}{\Gamma(a)\Gamma(b)}f_{bv}^{a-1}(1-f_{bv})^{b-1} \text{ with } f_{bv} = \frac{v(x')}{v(x)} \tag{3}$$

1.2. Identifiability analysis

This analysis aims to identify the operating conditions under which the parameters can be determined and to assess the robustness of these identifications to the experimental error (Loosdrecht et al, 2016). It involves three stages: first, parameter estimation is done using statistical and optimization algorithms within either the Frequentist (based on likely outcomes) or Bayesian (based on prior probability distributions) frameworks. Next, uncertainty is assessed using techniques like Markov Chain Monte Carlo (MCMC) to quantify impact of the estimates on model outputs. High parameter correlations can cause compensation effects, complicating unique estimations. Thus, the third step—sensitivity and identifiability analysis—identifies a subset of reliably

estimable parameters. This process is refined iteratively until the parameter set meets criteria such as a delta mean-square measure δ^{msqr} below 0.1 and a collinearity index between 10 and 15.

2. Results and discussion

Both of the optimization methods (Frequentist and Bayesian) converge to the same parameter values indicating that the measurements are distributed with a white Gaussian noise. The standard deviation and relative error of estimates were under 10 %, indicating good estimation.

However, the high correlation of B_1 with B_2 and B_3 (Table 1) suggests the need for identifiability analysis. This can also be addressed by increasing the information content (range of operating conditions), selecting a subset of parameters that is identifiable with the available data, or switching models.

Figure 1 illustrates the δ^{msqr} ranking of the three parameters under different conditions. It is observed that at low dispersed viscosities, the significance of the term B_3 diminishes, suggesting that under such conditions it can be omitted from the probability function. It Is however important to note that in the probability kernel, the B_2 term is divided by $\varepsilon^{2/3}$ while the B_3 term is divided by $\varepsilon^{1/3}$. This means that at lower energy dissipation (e.g. in a stirred tank) the B_3 term should be kept in the kernel even for lower dispersed phase viscosities.

Table 1. *Parameter estimation results obtained with Coulaloglou and Tavlarides model.*

	Estimate [B_1, B_2, B_3]	**Standard Deviation**	**Correlation Matrix**			
				B1	**B2**	**B3**
Bayesian	[0.0186, 0.4428, 0.3464]	[1E-4, 2.7E-3, 1.8E-3]	**B1**	1		
			B2	**0.5462**	1	
			B3	**0.7435**	0.0594	1

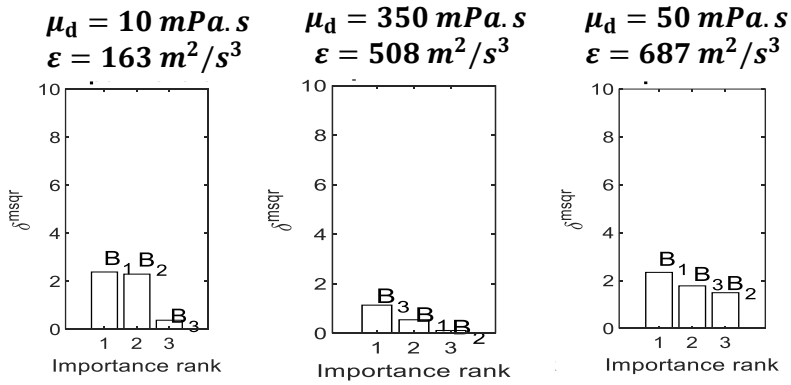

Figure 1. *Significance ranking of the δ^{msqr} for the three parameters across three different experiments.*

3. Conclusion

In this research, parameter identifiability and uncertainty analysis were applied to PBM for two breakage kernels. The methodology helps determine the identifiable set of parameters in a specific range of operating conditions. This is useful for its implementation in various applications and scales.

REFERENCES

Lebaz, N. *et al.* (2024) *Chemical Engineering and Processing - Process Intensification*, 199, p. 109770. https://doi.org/10.1016/j.cep.2024.109770.

Loosdrecht, M.C.M. van, Nielsen, P.H., Lopez-Vazquez, C.M., Brdjanovic, D. (Eds.), 2016. IWA Publishing, London. https://doi.org/10.1016/j.ces.2023.119688.

2nd Population Balance Modeling Webinar
25th November 2024, online

Modelling controlled drug release from Pickering emulsions made with flavonoid crystals

Pierfrancesco Latorre[1], G. Del Duca[1], A. Buffo[1], E. Simone[1]

[1]Department of Applied Science and Technology, Politecnico di Torino, Torino, Italy
Corresponding author email: pierfrancesco.latorre@polito.it

Keywords: Pickering; Emulsions; Model; PBM; Curcumin

ABSTRACT

Pickering emulsions, stabilized by solid particles at the oil-water interface, have gained attention due to their advantages over traditional surfactant-stabilized emulsions. The high desorption energy of solid particles results in nearly irreversible interfacial adsorption, enhancing stability. Additionally, biocompatible materials can be used as surfactants or tailored for specific functions (Sun et al., 2022). Crystalline particles, especially polyphenol crystals, are promising for stabilizing interfaces and providing functional properties like controlled release, making them suitable for pharmaceuticals, food, and cosmetics (Zembyla et al., 2018). A model was developed, capable of describing a water-in-oil Pickering emulsion system stabilized by curcumin crystals. The water droplets contain an active ingredient that is released into the oil when the crystals dissolve, as the exchange surface between the two phases increases. To correctly account for the presence of a crystal population, described by an assumed log-normal distribution, a Population Balance model (PBM) was used. The terms for birth and death were not considered; instead, the variations over time are solely due to a negative growth rate representing the dissolution rate of the curcumin crystals:

$$\frac{\partial n(L)}{\partial t} + \frac{\partial}{\partial L}(G(L)n(L)) = 0$$

The chosen method for solving the PBEs is the quadrature method of moments (QMOM), with nodes calculated using the Wheeler algorithm.

$$\frac{\partial m_k}{\partial t} + kGm_{k-1}$$

The negative growth term, representing the dissolution rate of the crystals, was determined as shown below:

$$\begin{cases} \frac{dm}{dt} = \frac{d\rho V}{dt} = \rho k_v \frac{dL^3}{dt} = \rho k_v 3L^2 \frac{dL}{dt} \\ \frac{dm}{dt} = -k_m k_a L^2 \left(C_{bulk} - C_{solubility}\right) M \end{cases}$$

$$\frac{dL}{dt} = M \frac{k_m k_a}{k_v 3}(C_{solubility} - C_{bulk})$$

Where km is the mass-transfer coefficient, ka and kv are respectively the area and volume shape coefficient and ρ is the curcumin density. The driving force—the concentration difference—changes over time as the concentration of curcumin in the oil, Cbulk increases, thereby decreasing the dissolution rate. The results obtained from simulations, using initial data extrapolated from previous work conducted in the group (Del Duca et al., 2024), such as the mean diameter of water droplets and curcumin crystals, indicate that the model predicts plausible behaviour for the concentration of the active ingredient encapsulated in the

dispersed phase, in both the oil and water phases over time, as well as for the concentration of curcumin in the oil (Fig. 1).

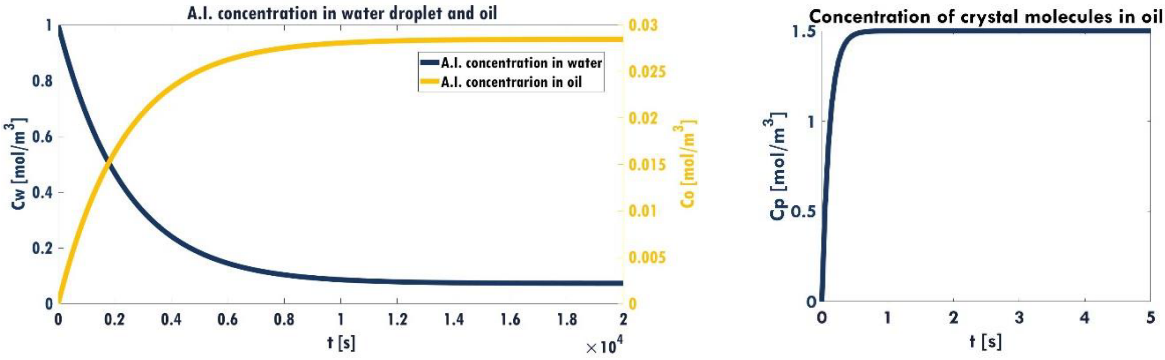

Fig 1 *Predicted concentration of Active Ingredient (left) and curcumin (right) in the two phases*

CONCLUSIONS

The next steps to be taken are the implementation of data from laboratory experiments into the model itself, this information have to be be integrated in the initial data of the model, such as the covering fraction values, a parameter able to tell how much of the droplets' interface is covered by the crystals. Also, a possible next important element to integrate into the model could be an experimental discrete population size distribution.
The model could also be implemented with the use of the extended method of moments to accurately account for the presence of the death terms.

REFERENCES

Sun, Z., Yan, X., Xiao, Y., Hu, L., Eggersdorfer, M., Chen, D., Yang, Z., & Weitz, D. A. (2022). Pickering emulsions stabilized by colloidal surfactants: Role of solid particles. In *Particuology* (Vol. 64, pp. 153–163). Elsevier B.V. https://doi.org/10.1016/j.partic.2021.06.004

Zembyla, M., Murray, B. S., & Sarkar, A. (2018). *Water-In-Oil Pickering Emulsions Stabilized by Water-Insoluble Polyphenol Crystals*. https://doi.org/10.1021/acs.langmuir.8b01438

2nd Population Balance Modeling Webinar
25th November 2024, online

Performance analysis and accuracy of numerical methods for solving simultaneous nonlinear particulate processes with multidimensional extension

Prakrati Kushwah[1], Jitraj Saha[1] and Andreas Bück[2]

[1]Department of Mathematics, National Institute of technology Tiruchirappalli, Tamil Nadu – 620 015, India
[2]Institute of Particle Technology, Friedrich-Alexander Universität Erlangen-Nürnberg, Erlangen - 91058, Germany

Corresponding author email: jitraj@nitt.edu

ABSTRACT

The simultaneous population balance equation (PBE) incorporating diverse particulate process aggregation, breakage, growth, nucleation and source is a long-standing and significant problem in the field of particulate sciences such as pharmaceutical industry, chemical engineering, astrophysics, biology etc. Due to the complex and non-linear nature of the governing equations, finding analytical solution is quite challenging for empirical kernels. In this work, simultaneous PBEs are solved using sectional and semi-analytical technique. The performance, adaptability and accuracy of both the methods for solving simultaneous PBEs are discussed in detail. Both the schemes are further extended to solve simultaneous PBE in multidimensions. Performance analysis is also executed for multidimensional models.

Keywords: Simultaneous population balance equation; Sectional methods; Homotopy analysis method; Convergence; Multidimensional models.

1. INTRODUCTION

The dynamic evolution of particle population within a system is described using a fundamental mathematical framework popularly known as population balance equation (PBE). The theoretical and numerical studies of PBEs provide a comprehensive description about the change in particle population and its properties over time. Such changes generally occur due to particulate processes such as aggregation, breakage, growth and nucleation etc. These processes have significant applications in various fields of science and technology. The PBE gives several insights of industrial and natural process. Moreover, Understanding the combined model of particulate processes is crucial for interpreting systems which involve multiple phases.

The PBE describing simultaneous aggregation, breakage, growth, nucleation and other sources is represented by an integro-partial differential equation and stated as

$$\frac{\partial n(t,x)}{\partial t} + \frac{\partial [G(t,x)n(t,x)]}{\partial x} = \frac{1}{2}\int_0^x C(x-y,y)n(t,x-y)n(t,y)dy - \int_0^\infty C(x,y)n(t,x)n(t,y)dy + \int_x^\infty b(x,y)S(y)n(t,y)dy - S(x)n(t,x) + N(x) + B_{src}(t,x),$$

associated with the initial condition $n(0,x) = n_0(x) \geq 0$, for all $x \in [0,\infty]$. The first term on the left hand side of the equation (1) is the time evolution of the particle density $n(t,x)$ of $x(\geq 0)$ size particles at time $t(\geq 0)$. The function $G(t,x)$ is the rate responsible for particle growth, $C(x,y)$ is the aggregation kernel, $b(x,y)$ denotes the breakage function, $S(x)$ is the selection function, $N(x)$ is the nucleation rate and source term is given by $B_{src}(t,x)$.

2. MATERIALS AND METHODS

Due to the wide scope and applications of PBEs, many researchers have attempted to find the analytical or numerical solution to these equations. However, PBEs are represented by integro-partial differential equations which are either hyperbolic or parabolic in nature. Consequently, these equations exhibit a significant degree of complexity and nonlinearity in particular when coupled with aggregation terms. In literature, several techniques such as method of characteristics, discrete element method (DEM), stochastic methods, method of moments, sectional methods, semi-analytical methods etc. are available.

Above mentioned methods are claimed to be very robust and versatile, however they also come with several limitations. Thus, we need a robust analytical technique for which limitations can be minimized without compromising the accuracy of the approximated solution. Therefore, in this work, we propose to use the cell average technique (CAT) and homotopy analysis method (HAM) for solving simultaneous PBEs. Through this study, we attempt to address the following questions:

1. To which extent these methods produce desirable accurate results without compromising the robustness?
2. How accurately these methods are able to solve simultaneous PBEs, that is, when PBE models include more than one particulate processes?
3. When more than one particle property is considered, what is the efficiency of these methods to solve them?

3. RESULTS AND DISCUSSION

For all the examples, two type of initial distributions are considered: i) exponential and ii) Gaussian initial distribution. These initial conditions have specific physical significance in population balance theory. This discussion contains six test problems, out of which first five are dedicated to one dimensional problems and last one is devoted to multidimensional PBEs. To validate the accuracy and efficiency of the methods HAM, HPM and CAT, the numerical particle density and different order moments are compared. Here, we present results for the case where simultaneous aggregation, breakage, growth and source process are considered with Gaussian initial condition.

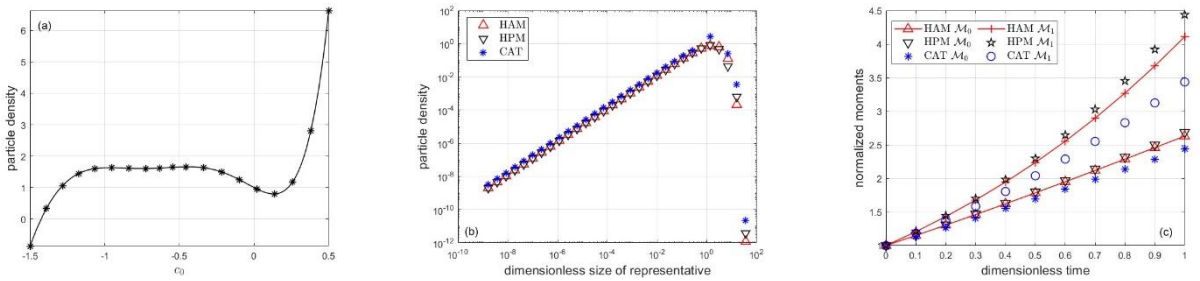

Figure 1: (a) c_0 −curve, (b) comparison of number densities and (c) moments for simultaneous process.

4. CONCLUSIONS

A comparative study is conducted to evaluate the performance of numerical techniques for solving simultaneous population balance models that incorporates various particulate processes simultaneously for sectional and semi analytical methods. A thorough investigation effectively tackled the obstacles

encountered in solving simultaneous PBEs. Overall, It was observed that HAM outperforms CAT in terms of reliability and accuracy. The HAM and CAT approach are extended for solving multidimensional models. HAM is more robust to be expandable in higher dimensions as compared to CAT.

REFERENCES

Ramkrishna, D. Population balances: Theory and applications to particulate systems in engineering. Academic Press, 2000. DOI: https://doi.org/10.1016/B978-0-12-576970-9.X5000-0

Kumar, J., Peglow, M., Warnecke, G. and Heinrich, S. An efficient numerical technique for solving population balance equation involving aggregation, breakage, growth and nucleation. Powder Technology, 182(1), pp.81-104, 2008. DOI: https://doi.org/10.1016/j.powtec.2007.05.028

Kushwah, P. and Saha, J. Improved accuracy and convergence of homotopy-based solutions for aggregation–fragmentation models. Mathematical Methods in the Applied Sciences, 46(6), pp.7180-7200, 2023. DOI: https://doi.org/10.1002/mma.8963

2nd Population Balance Modeling Webinar
25th November 2024, online

Population Balance Modelling for Gypsum Crystals in the Presence of Succinic Acid

Asu Deniz Kasap[1] and Sevgi Polat[1]

[1]Chemical Engineering Department, Faculty of Engineering, University of Marmara, İstanbul, Turkey
Corresponding author email: asu.deniz@marun.edu.tr

ABSTRACT

Calcium sulfate dihydrate (gypsum) is one of the most common minerals in nature and is widely used in environmental and chemical processes. Different crystalline morphologies of gypsum can have very different physical and chemical properties, which gives them great potential for crystal material applications. Therefore, crystalline morphological control of gypsum has become a hot topic in scientific research in recent years. Researchers established morphological control of gypsum by using various impurities and additives. This article investigated the effects of succinic acid used as an additive on gypsum crystallization. The experiments were performed in a mixed-suspension mixed-product removal (MSMPR)-type crystallizer at different succinic acid concentrations through the reaction of calcium carbonate solution with sulfuric acid solution. The crystal size distributions were measured, and the average particle size of gypsum were decreased in the presence of succinic acid when compared to the pure media. The kinetics of crystal growth of gypsum crystals were analyzed based on McCabe's ΔL law and the kinetic parameters were evaluated by the use of size-independent and size-dependent growth models using population balance theory. It has been found that the growth rate of crystals depends on the particle size, which was specified using ASL, C-R, MJ2, and MJ3 size-dependent growth models. Figure 1 shows the linear regression between population density ln (n) and crystal size (L) and the relationship of the estimations of different models with experimental data. Results demonstrated that the MJ3 model was found to be the best model to characterize the experimental data with a high relative coefficient. The presence of succinic acid also led to a decrease in the growth rate of gypsum crystals.

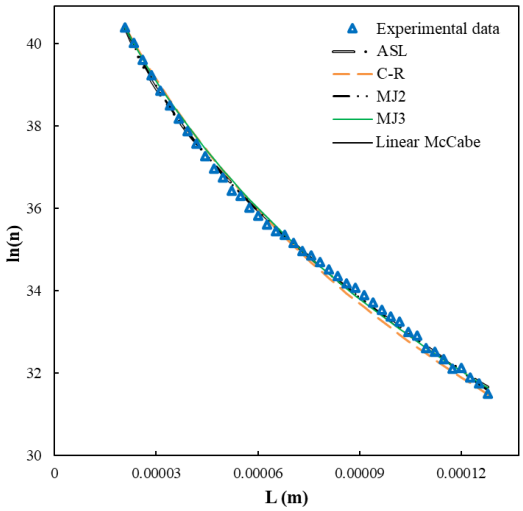

Figure 1. *Population density evaluation according to the size-independent and size dependent models for gypsum crystals.*

Keywords: Gypsum; kinetics; crystallization; additive.

2nd Population Balance Modeling Webinar
25th November 2024, online

Integrated Liquid-Liquid Extraction and Settler Model using PBM-HMMC in the Presence of Surfactant

Mahdi Mousavi, Ville Alopaeus[1]

[1]Department of Chemical and Metallurgical Engineering
Corresponding author email: mahdi.mousavi@aalto.fi

ABSTRACT

This research presents a two-step process for liquid-liquid extraction and phase separation, focusing on the role of surfactants and droplet behavior in emulsions. It employs a high-order moment-conserving method of classes based population balance method (PBM-HMMC) to model single-stage extraction and gravitational phase separations of batch oil-water emulsions. The study examines the effects of surfactants on droplet interactions, size distribution, coalescence and breakage. Surfactants inhibit coalescence and form microemulsions, increasing surface area for mass transfer and enhancing extraction efficiency, but they also stabilize emulsions, making phase separation more difficult. Thus, a trade-off exists between extraction efficiency and phase separation when surfactants are present. Although the model has yet to be validated against experimental data, it aligns with theoretical principles and offers reasonable predictions based on current system understanding.

Keywords: Liquid-Liquid Extraction; Gravitational Phase Separation; Surfactants; Population Balance Modeling (PBM); Emulsion Stability.

1. Introduction

In liquid-liquid dispersion of two immiscible liquids, the population balance method (PBM) effectively tracks droplet behavior and size evolution under varying conditions (Lebaz and Sheibat-Othman, 2022). This approach is often applied to non-homogeneous systems like stirred tanks and settlers to model droplet breakage and coalescence. However, many models overlook the role of surfactants, which stabilize emulsions by preventing droplet coalescence (**Figure 1**), improving mass transfer but complicating phase separation (Alopaeus, 2022, Mousavi et al., 2024). This study integrates high-order moment-conserving method of classes (HMMC) based PBM with coalescence closure to predict how surfactant concentration and type affect the process. Additionally, a settler model based on Stokes' law accounts for droplet-droplet and droplet-interface coalescence, providing insights into surfactant effects and predicting separation behavior at various concentrations.

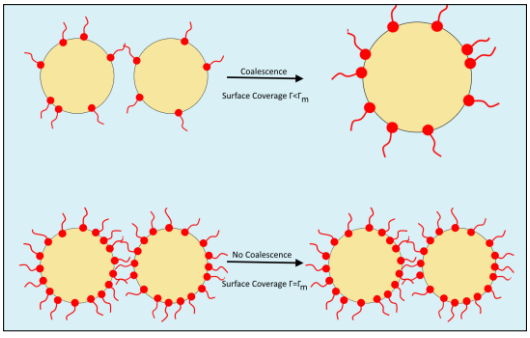

Figure 1. Visual representation of droplet-droplet coalescence processes in an emulsion due to surfactant, highlighting the interaction dynamics between surfactant and droplet interface (Mousavi et al., 2024).

2. Population Balance Model

In this work the population balance model is used to predict the droplet-droplet coalescence behavior and calculating the available surface area for surfactant. It can be expressed as:

$$\frac{dY_i}{dt} = B_C - D_C + B_D - D_D + S \qquad (1)$$

Y represents the droplet numbers within a specific category (*i*). B_c, D_c, B_B and D_B are the birth and death terms due to coalescence and breakage (subscripts), while *S* is a sink term accounting for droplets removed due to droplet-interface coalescence in phase separation process. Detailed formula derivations and system closures, including mass transfer, creaming, coalescence, and dense-packed zone interface height, are thoroughly presented in Alopaeus, 2022 and Mousavi et al., 2024.

3. Results and Discussions

This section explores the impact of varying surfactant concentrations on liquid-liquid extraction and phase separation, testing levels of 0, 0.1, 0.2, and 0.3 mol/m³. The results show that increasing surfactant concentration changes the droplet size distribution, leading to more available surface area for mass transfer and prolonging phase separation time, as higher levels of surfactant stabilize emulsions by preventing droplet coalescence. Without surfactant, separation occurs quickly, but at higher concentrations, surface coverage increases, reducing droplet size and enhancing the stability of emulsion. **Figure 2** illustrates how surfactants and surface coverage increase extraction efficiency, delay phase separation and reduce droplet size, aligning with the Langmuir isotherm, which suggests that surface coverage increases with surfactant concentration until saturation.

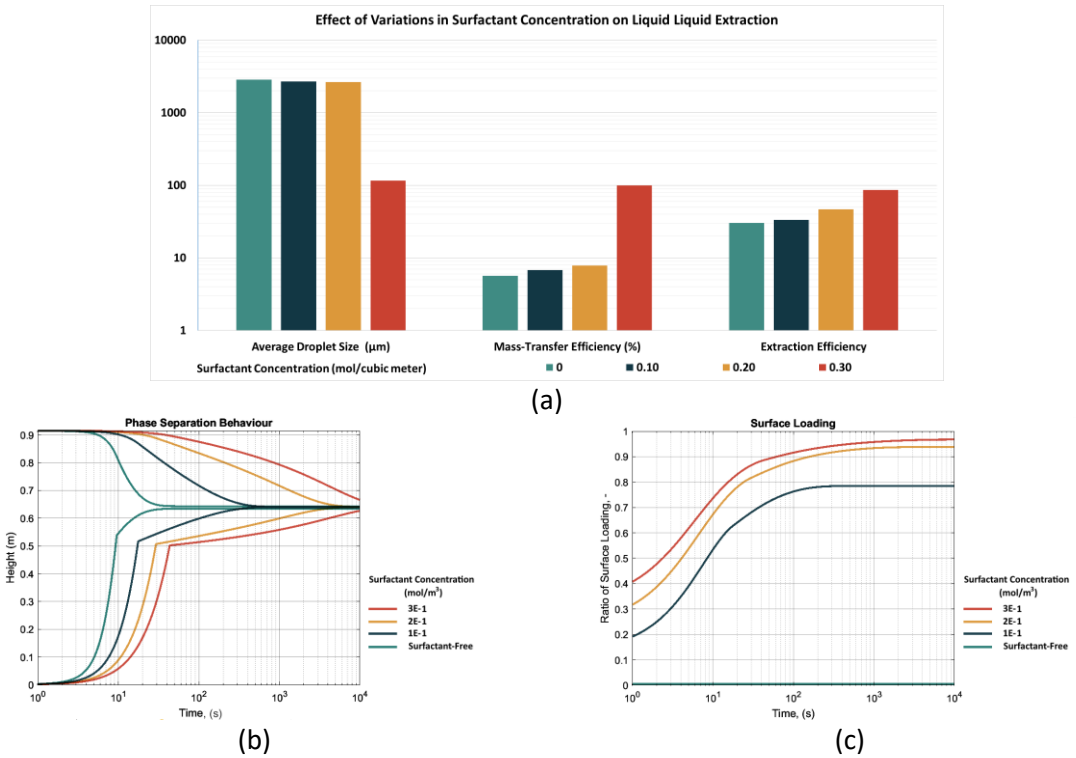

Figure 2. Depiction of liquid-liquid extraction and phase separation behavior at varying surfactant concentrations. **(a)** The average droplet size, mass-transfer and extraction efficiency in liquid-liquid extraction model. **(b)** Phase separation profile vs time in settler. **(c)** Surfactant surface loading in settler.

REFERENCES

ALOPAEUS, V. 2022. Modeling surfactant and drop size dynamics in polydisperse liquid-liquid systems with population balances. *Chemical Engineering Science,* 248**,** 117269.

LEBAZ, N. & SHEIBAT-OTHMAN, N. 2022. Population balance modelling of a continuous static mixer-based emulsification process. *Chemical Engineering Research and Design,* 188**,** 645-654.

MOUSAVI, M., BERNAD, A. & ALOPAEUS, V. 2024. Modeling oil/water emulsion separation in batch systems with population balances in the presence of surfactant. *Chemical Engineering Science,* 300**,** 120558.

2nd Population Balance Modeling Webinar
25th November 2024, online

A novel theoretical breakup model considering energy consumption during eddy-bubble interaction

Xu-Qing Wang, Xi-Bao Zhang* and Zheng-Hong Luo*

Department of Chemical Engineering, School of Chemistry and Chemical Engineering, State Key Laboratory of Metal Matrix Composites, Shanghai Jiao Tong University, Shanghai 200240, P. R. China
Corresponding author email: 13127935995@sjtu.edu.cn
Corresponding author email: luozh@sjtu.edu.cn

ABSTRACT

This work aims to develop a bubble breakup model that includes the impact of energy consumption during the eddy-bubble collision/interaction, which significantly affects bubble breakup and is normally neglected in previous studies. To establish an improved breakup model, the collision angle θ and the interaction angle δ are adopted to accurately quantify the energy consumption during the collision between smaller eddies and bubbles, and the interaction between larger eddies and bubbles, respectively. Generally, energy consumption leads to lower breakup frequency and breakup rate. The developed model can be applied to precisely predict bubble breakup rate and daughter size distribution under various conditions.

Keywords: bubble breakup model; energy consumption; collision angle; interaction angle; population balance model.

1. Introduction

The population balance model (PBM) can give a prediction for bubble size distribution in gas-liquid reactors, which has much influence on the mass and heat transfer process (Shu et al., 2019). The model includes coalescence model and breakup model. In the breakup model, eddies with a size smaller than the mother bubble collide with the bubble, and those with a size larger than the mother bubble interact with the bubble. When the breakage criteria are satisfied, bubble breakage will occur. In this study, the energy consumption during the collision/ interaction process is considered. The collision angle θ and the interaction angle δ are used to quantify the consumption. The novel theoretical model is applied to predict the bubble breakup rate and daughter size distribution. The influence of the bubble size and turbulence tensity on the daughter size distribution are investigated.

2. Materials and methods

2.1. Collision/ Interaction frequency

Based on the analogy with gas kinetic theory, the collision frequency between bubbles and eddies with the size of $\lambda \le d$ is expressed as Equation 1(Luo and Svendsen, 1996). Andersson and Andersson (2006) stated that eddies with the size of $d \le \lambda \le 3d$ could also interact with the bubbles and bring about bubble breakage. In this work, the interaction frequency (as Equation 2) is set proportional to the volume of a bubble with a size of $0.5d_1$.

$$\omega_{\text{collision}} = 0.923\left(1-\alpha_d\right)\dot{n}\varepsilon^{1/3}\frac{\left(d+\lambda\right)^2}{\lambda^{11/3}} \qquad \left(\lambda \le d\right) \tag{1}$$

$$\omega_{\text{interaction}} = 0.0538\left(1-\alpha_d\right)\dot{n}\varepsilon^{1/3}\frac{d_1^3}{\lambda^{14/3}} \qquad \left(d < \lambda \le 3d\right) \tag{2}$$

2.2. Breakage criteria

The surface energy criterion and the force criterion are used to constrain the bubble breakage in this work. It means that only if the energy provided by the eddy exceeds the surface energy increase during bubble breakage $\chi_{c,s} = \Delta e_\sigma\left(d, f_v\right)/\overline{e}_{\text{avail}}\left(\lambda\right) \le 1$, and meanwhile the inertial force exerted on the bubble exceeds the surface tension force $\chi_{c,f} = \tau_\sigma/\overline{\tau}_{\text{avail}} \le 1$, bubble breakage occurs.

The increase in surface energy during bubble breakage is calculated by,

$$\Delta e_\sigma\left(d, f_v\right) = \left[f_v^{2/3} + \left(1-f_v\right)^{2/3} - 1\right]\pi d^2\sigma \tag{3}$$

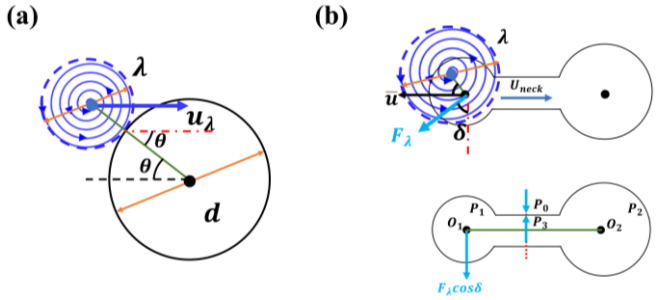

Figure 1. *Schematic diagram of (a) smaller eddy-bubble collision, and (b) larger eddy-bubble interaction*

As shown in **Figure 1**, the available energy that transfers from an eddy to a bubble is expressed as,

$$\bar{e}_{\text{avail}}(\lambda)=\begin{cases}(\pi/12)\rho_l\bar{u}^2_{\text{avail}}(\lambda\cos\theta)^3=(\pi/12)\rho_l\bar{u}^2_\lambda\lambda^3\left[1-\cos(0.5\pi\cos\theta)\right]^2\cos\theta & (\lambda\le d)\\ (\pi/12)\rho_l\lambda^3\bar{u}^2_{\text{avail}}=\pi\rho_l\bar{u}^2_\lambda\lambda^3\left[1-\cos\left(0.5d_1\pi/\lambda\right)\right]^2/(12d_1^2) & (d<\lambda\le 3d)\end{cases} \tag{4}$$

The interfacial force needs to be overcome by eddies in the breakup process can be calculated as,

$$\tau_\sigma=\begin{cases}\sigma/d_1 & (\lambda\le d)\\ \sigma/d_{\text{neck}} & (d<\lambda\le 3d)\end{cases} \tag{5}$$

It can also be known from **Figure 1** that the inertial force cannot fully act on the bubble. The available inertial force exerted on the bubble is expressed as,

$$\bar{\tau}_{\text{avail}}=\begin{cases}0.5\rho_l\bar{u}^2_{\text{avail}}=0.5\rho_l\bar{u}^2_\lambda\left[(1-\cos(0.5\pi\cos\theta))/\cos\theta\right]^2 & (\lambda\le d)\\ F+P_0-P_3=\bar{F}_\lambda\cos\delta\dfrac{(d_1+d_2)/2+l_{neck}}{(l_{neck}+d_2)/2}+\dfrac{1}{2}\rho_g u^2_{\text{neck}}+\dfrac{1}{2}\zeta_c\rho_g u^2_{\text{neck}}+\dfrac{4\mu_g l_{\text{neck}}u_{\text{neck}}}{(d_{\text{neck}}/2)^2}-\dfrac{4\sigma}{d_1} & (d<\lambda\le 3d)\end{cases} \tag{6}$$

$$\bar{F}_\lambda=\begin{cases}\dfrac{1}{d_1}\int_{\lambda/2-d_1}^{\lambda/2}\dfrac{\sqrt{2}}{2}\pi^2\varepsilon^{1/3}\lambda^{-2/3}\mu_1\cos\dfrac{\pi}{\lambda}x\,dx & \dfrac{\lambda}{2}\le d_1\\ \dfrac{1}{d_1-\lambda/2}\int_{\lambda-d_1}^{\lambda/2}\dfrac{\sqrt{2}}{2}\pi^2\varepsilon^{1/3}\lambda^{-2/3}\mu_1\cos\dfrac{\pi}{\lambda}x\,dx & \dfrac{\lambda}{2}>d_1\end{cases} \tag{7}$$

2.3. Breakage probability, breakup frequency, and daughter bubble size distribution

Combining those two breakage criteria, the breakage probability can be calculated as,

$$P_B\left(f_v|\ d,\lambda\right)=1-\int_0^{\chi_c}\exp(-\chi)d\chi=\exp(-\chi_c)=\exp\left(-\max(\chi_{c,s},\chi_{c,f})\right) \tag{8}$$

The total bubble breakup rate $\Omega(d)$, the breakup frequency $\mathrm{b}(d)$, and the daughter bubble size distribution $\beta(f_v,d)$ are described as Equations (9) to (11), respectively.

$$\Omega(d)=\int_0^{0.5}\int_{11.4\eta}^{3d}P_B\left(f_v|\ d,\lambda\right)\omega_\lambda(d)\mathrm{d}\lambda\mathrm{d}f_v \tag{9}$$

$$b(d)=\Omega(d)/n \tag{10}$$

$$\beta(f_v,d)=\frac{\int_{11.4\eta}^{3d}P_B\left(f_v|\ d,\lambda\right)\omega_\lambda(d)\mathrm{d}\lambda}{\Omega(d)} \tag{11}$$

3. Results and discussion

3.1. Bubble breakup frequency

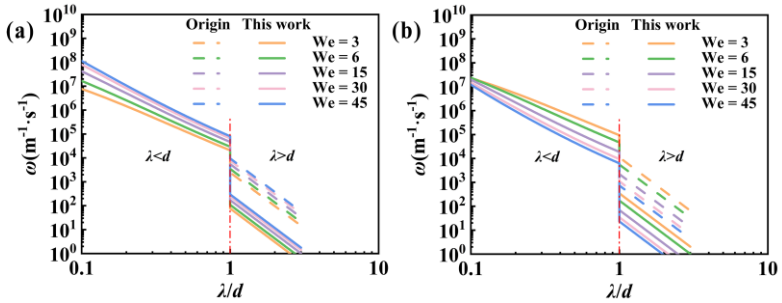

Figure 2. *Collision/ Interaction frequency of dimensionless eddy scale with (a) the same mother bubble size (d = 4 mm), and (b) the same turbulent dissipation rate ($\varepsilon = 5\,m^2/s^3$).*

Herein, the effect of the interaction volume on the interaction frequency is shown in **Figure 2**. The influence of the turbulence tensity and the bubble scale are illustrated in **Figures 2**(a) and (b), respectively.

3.2. Breakup rate and daughter size distribution

The predicted dimensionless breakup rate is compared with experiment results (Krishna et al., 1991; Martínez-Bazán et al., 1999; Vejražka et al., 2018; Zednikova et al., 2019; Zhang et al., 2023), as shown in **Figure 3**(a). The prediction results of this work are in accordance with the experimental data from Vejražka et al. (2018). The predicted daughter size distribution is compared with the DNS results from Rivière et al. (2021), as seen in **Figure 3**(b). The influence of the *We* number, which represents the bubble size or fluctuation tensity, on the daughter size distribution is also shown in **Figure 3**(b).

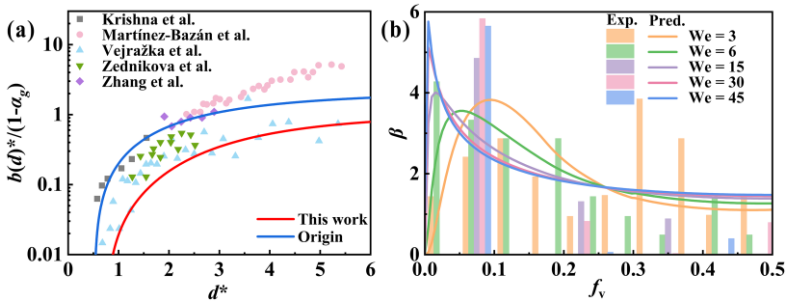

Figure 3. *Comparison of predicted and measured (a) dimensionless bubble breakup rate and (b) daughter size distribution.*

4. Conclusions

Energy consumption during the eddy-bubble collision/ interaction is pointed out and considered in the bubble breakup model derivation. The surface energy criterion and force criterion are considered to constrain the bubble breakup. The conclusions obtained in this work are as follows: a) With the addition of θ , the bubble breakup probability becomes lower. b) The new model proposed is applicable for the prediction of bubble breakup in a bubble column. c) With the increase of the turbulence tensity, bubbles tend more to break up equally, though most bubbles still tend to break into two daughter bubbles with unequal volume.

REFERENCES

Andersson, R., Andersson, B., 2006. Modeling the breakup of fluid particles in turbulent flows. *AIChE J.*, 52, 2031-2038.

Krishna, R., Wilkinson, P.M., Van Dierendonck, L.L., 1991. A model for gas holdup in bubble columns incorporating the influence of gas density on flow regime transitions. *Chem. Eng. Sci.*, 46, 2491-2496.

Luo, H., Svendsen, H.F., 1996. Theoretical model for drop and bubble breakup in turbulent dispersions. *AIChE J.*, 42, 1225-1233.

Martínez-Bazán, C., Montañés, J.L., Lasheras, J.C., 1999. On the breakup of an air bubble injected into a fully developed turbulent flow. Part 1. Breakup frequency. *J. Fluid Mech.*, 401, 157-182.

Rivière, A., Mostert, W., Perrard, S., Deike, L., 2021. Sub-Hinze scale bubble production in turbulent bubble break-up. *J. Fluid Mech.*, 917, A40.

Shu, S., Vidal, D., Bertrand, F., Chaouki, J., 2019. Multiscale multiphase phenomena in bubble column reactors: A review. *Renew. Energy*, 141, 613-631.

Vejražka, J., Zedníková, M., Stanovský, P., 2018. Experiments on breakup of bubbles in a turbulent flow. *AIChE J.*, 64, 740-757.

Zednikova, M., Stanovsky, P., Travnickova, T., Orvalho, S., Holub, L., Vejrazka, J., 2019. Experiments on Bubble Breakup Induced by Collision with a Vortex Ring. *Chem. Eng. Technol.*, 42, 843-850.

Zhang, H., Wang, Y., Sayyar, A., Wang, T., 2023. Experimental study on breakup of a single bubble in a stirred tank: Effect of gas density and liquid properties. *AIChE J.*, 69, e17511.

2nd Population Balance Modeling Webinar
25th November 2024, online

Population Balance Modeling of Crystallization Processes for Efficient Metal Recovery from Spent Batteries

Vandana Kumari Jha[1] and Christophe Duwig[1]

[1]Department of Chemical Engineering, KTH Royal Institute of Technology, Stockholm, Sweden
Corresponding author email: vkjha@kth.se

ABSTRACT

The increasing demand for electric vehicles and energy storage systems has led to an increase in battery production, consequently generating a growing volume of spent batteries. To address the environmental and economic challenges associated with battery waste, efficient and sustainable recycling processes are crucial. This study focuses on developing a population balance model (PBM) to simulate and optimize metal recovery from spent batteries through crystallization. In the context of battery recycling, crystallization offers a promising approach for recovering valuable metals. The population balance equation (PBE) provides a comprehensive framework for understanding and predicting particle size distribution (PSD) in crystallization process. This study focuses on developing a PBM to simulate and optimize the crystallization process for metal recovery. This model solves a discretized formulation of the PBE to obtain the crystal size distribution from crystallization of nickel sulfate in a 3D T-mixer.

Keywords: population balance model; metal recovery; battery recycling; crystallization; particle size distribution.

1. Introduction

As our society is moving towards electrification the demand for energy storage solutions such as batteries is on the rise. Lithium-ion batteries, while essential for energy storage, pose significant recycling challenges due to scarcity and valuable constituent metals. To achieve a circular economy and sustainable use of batteries, novel and improved recycling processes need to be developed. Crystallization, a proven technique for purifying and separating substances, emerges as a promising approach for recovering valuable metals from spent batteries. In a crystallisation process, crystal population can be described by its size distribution which gives information regarding the number of crystals at certain particle sizes/volumes. Particle size distribution (PSD) significantly impacts the product quality, with factors such as filterability, solubility, and purity getting influenced by it. To optimize product characteristics, precise control and prediction of PSD are essential.

The population balance equation (PBE) is a powerful mathematical tool for describing the evolution of particle populations. By incorporating nucleation, growth, aggregation, and breakage, the PBE provides a comprehensive framework for understanding PSD. This necessitates advanced simulation tools capable of accurately capturing the complex interplay of these phenomena. By considering thermodynamic and kinetic factors, crystal size and shape distributions is predicted, enabling effective process design and control.

This work focuses on applying the PBE, coupled with the computational fluid dynamics (CFD), to simulate the evolution of particle population in a continuous reactor configuration. A 3D T-mixer is employed to investigate the impact of reactor hydrodynamics on nickel sulfate crystallization (Schwarzer and Peukert, 2004; Tang et al., 2022). By understanding the underlying mechanisms governing growth kinetics, this research aims to contribute to the development of advanced crystallization processes for improved product quality, higher yields, and reduced energy consumption, particularly in the context of battery recycling.

2. Model definition

The approach presented in this report implements discretization as the chosen method for solving the PBE (Qamar et al., 2006). The PBE is discretized into *i* intervals as given by Equation 1.

$$\frac{\partial n}{\partial t} + \nabla.(un) + \frac{\partial(G(S,L))n(L)}{\partial L} = \frac{\nu}{Sc}\nabla^2 n + B_{nuc}\delta(L - L_{C_0}) + B_{agg} - D_{agg} \quad (1)$$

Geometric grid method is implemented to discretise the internal coordinate of the PBE (Equation 2).

$$L_j = L_{min} + 2^{\frac{(j-N)}{q}}(L_{max} - L_{min}) \quad (2)$$

The described numerical approach is applied to simulate crystallization within a 3D tubular T-mixer, characterized by defined geometry and inlet conditions, at a Reynolds number of 255 (Figure 1(a)). Nucleation and breakage are not considered in the model; instead, seeds are introduced with a starting particle size of 7.8 µm. Crystal growth (G) is described by a simplified size-independent power-law model, where g and k_g are fitted parameters, with the final model expressing crystal growth as a function of supersaturation (S) at 25°C given as

$$G = g(S-1)^{k_g} * 10^{-8} \quad (3)$$

The crystallization reaction is modelled with Chemistry interface and PBE is solved using Stabilized Convection-Diffusion equations in 3D, with additional source terms for growth. The numerical approach is implemented using COMSOL Multiphysics® version 6.2.

3. Results and discussions

The flow field exhibited significant mixing, with the flow initially dividing into quadrants before becoming more uniform along the channel length (Figure 1(b)-(c)). Supersaturation profiles revealed an even distribution along the channel length in 3D model, resulting in a narrower crystal size distribution at the outlet (Figure 1(d)). Supersaturation values were higher, potentially due to enhanced mixing efficiency. The corresponding crystal size distribution exhibited local regions of larger crystals within the mixing zone, reflecting the spatial variations in supersaturation. These findings highlight the importance of considering 3-D effects for accurate prediction of crystal size distribution in T-mixer systems.

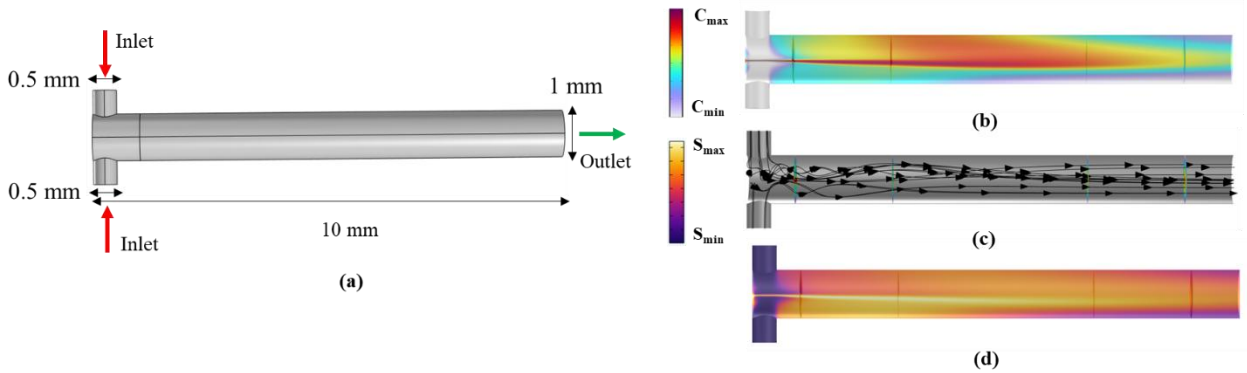

Figure 1. a) *Geometry for the 3D T-mixer;* contour plots shown at a center cut plane inside the T-mixer (Re = 255): b) nickel sulfate crystallization, c) streamline plot, and d) supersaturation.

REFERENCES

H.C. Schwarzer and W. Peukert, "Combined experimental/numerical study on the precipitation of nanoparticles," *AICHE J.*, vol. 50, no. 12, pp. 3234–3247, 2004.

H. Y. Tang, S. Rigopoulos, and G. Papadakis, "On the interaction of turbulence with nucleation and growth in reaction crystallisation," *J. Fluid Mech*, vol. 944, p. A48, 2022.

S. Qamar, M.P. Elsner, I.A. Angelov, G. Warnecke and A. Seidel-Morgenstern, “A comparative study of high resolution schemes for solving population balances in crystallization,” *Comput. Chem. Eng.*, vol. 30, no. 6–7, pp. 1119–1131, 2006.

2nd Population Balance Modeling Webinar
25th November 2024, online

Investigation of Kinetics in Crystallization of Lactose: Model development and parameter estimation

Ramona Bier[1], Sanharpoth Petchmunee[1], Heiko Briesen[1]

[1]School of Life Sciences, TU Munich, Freising, Germany
Corresponding author email: ramona.bier@tum.de

ABSTRACT
Batch cooling crystallization is a crucial step in lactose production, a key ingredient in pharmaceuticals and many food products. This study presents an investigation of the kinetics involved. A one-dimensional population balance model is employed to track the time-dependent evolution of lactose crystals. The kinetic parameters for the crystallization process are estimated based on experimental data using process analytical technology (PAT). Growth, nucleation, and agglomeration kinetics are estimated. To accurately track concentration depletion, respectively growth, in the presence of agglomeration a reduced order model is developed. Within this model reduction, surface area development is tracked separately in a second population balance. The model demonstrates a significant improvement in aligning experimental results with simulations compared to a basic one-dimensional population balance model.

Keywords: population balance model, model reduction, crystallization, parameter estimation

1. Introduction

Lactose crystallization has been practiced for over a century (Paterson 2009). However, a detailed understanding of this process is still lacking despite its long history. One reason for this knowledge gap is the varied initial compositions involved. Lactose can be crystallized from whey or whey permeate, derived from sweet or acidic whey, or even from almost pure water for pharmaceutical recrystallization (Paterson 2009). Moreover, the crystallization encompasses multiple simultaneous processes, including nucleation, growth, aggregation, and mutarotation. The latter is unique to some organic sugars, like lactose, as it exists in two anomeric forms, with only one form crystallizing during the cooling crystallization process. These anomers can interchange in solution through an equilibrium reaction known as mutarotation. In this study, we utilize a population balance framework to develop a model for lactose crystallization.

2. Methods

A one-dimensional population balance (1D) model with particle volume as the characteristic variable describes crystal evolution, assuming a perfectly mixed batch reactor, no growth-rate dispersion, and negligible breakage. Mass balances connect the liquid concentrations of α- and β-lactose with the population balance and consider mutarotation. The model accounts for growth, mutarotation, nucleation, and agglomeration kinetics. However, in a 1D population balance, the surface area of agglomerated particles is smaller than the sum of the surface areas of the primary particles, as only volume is conserved. In systems with significant agglomeration, this leads to under-predicting concentration depletion (Kovačević and Briesen 2019). To address this, a two-dimensional population balance could be used to preserve surface area, but this comes with a significantly higher computational cost. Instead, a novel reduced-order model consisting of two 1D population balances is applied. The first PBM tracks the evolution of the number density distribution, while the second PBM tracks the area density distribution, ensuring that the surface area of the primary particles is conserved during agglomeration (see Figure 1). The necessary kinetic parameters for the crystallization process were obtained through parameter estimation, minimizing the sum of squared residuals between experimental and simulation data.

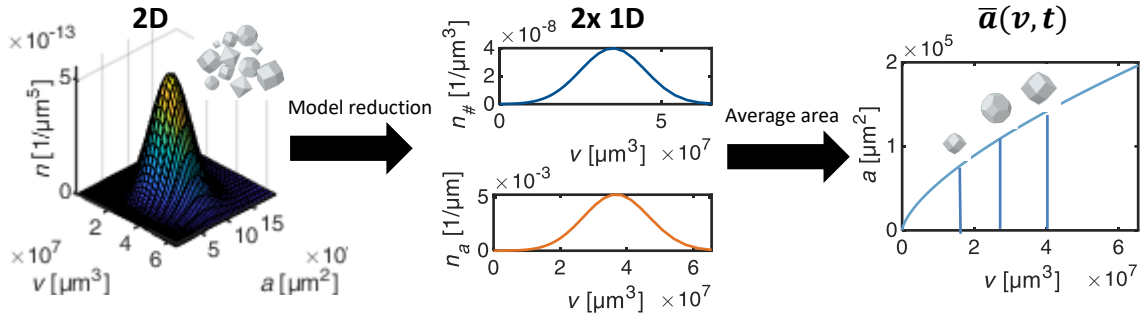

Figure 1. *Scheme showing the model reduction from 2D to two 1D population balances providing average area data* $\bar{a}(v,t)$

3. Results and discussion

Various kinetic expressions for secondary nucleation and agglomeration were evaluated during the model development and parametrization process. While incorporating agglomeration into the 1D population balance model (PBM) improved the model's fit to experimental data, it also overestimated the final lactose concentration in the solution. This overestimation arises because the 1D PBM conserves particle volume during agglomeration but not surface area. In contrast, the reduced-order model preserves the total surface area of the original particles during agglomeration. This implies that the crystals are assumed to fuse at a single point instead of fully coalescing. The improvement in model accuracy is demonstrated in Figure 2, which compares the standard 1D PBM solution with the adapted 1D PBM simulation. The final concentration predicted by the adapted model aligns closely with the experimental results, whereas the standard model overestimates the final concentration by 14%. Additionally, the alignment of the final volume density distribution is improved.

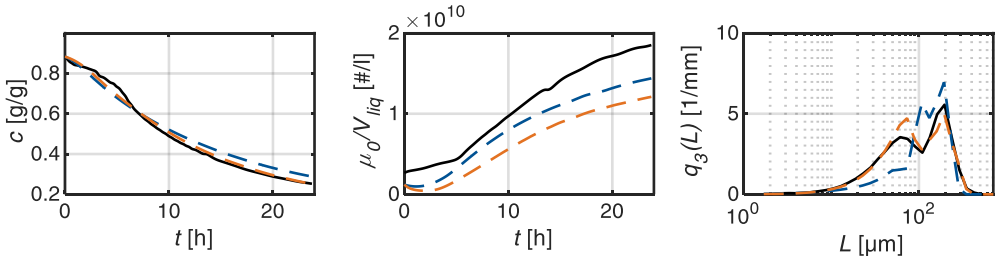

Figure 2. *From left to right: Lactose load* c*, particle density* μ_0/V_{liq} *over time* t *and normalized final volume density distribution* $q_3(L)$ *as measured in the experiment (line) and calculated by simulation (dashed) with the standard PBM (blue) and the adapted PBM (orange) for one exemplary crystallization experiment*

4. Conclusions

In conclusion, this study presents a comprehensive model for lactose crystallization that accurately captures the key processes: nucleation, growth, mutarotation, and agglomeration. Introducing a reduced-order model significantly improves the accuracy of simulations, aligning closely with experimental data. This model enhances our understanding of lactose crystallization and provides a solid foundation for optimizing industrial crystallization processes.

References

Kovačević, Tijana; Briesen, Heiko (2019): Simulations of crystal aggregation and growth: Towards correct crystal area. In *AIChe Journal* 65 (5), Article e16525. DOI: 10.1002/aic.16525.

Paterson, A. H. J. (2009): Production and Uses of Lactose. In Paul McSweeney, Patrick F. Fox (Eds.): Advanced Dairy Chemistry. New York, NY: Springer New York, pp. 105–120.

2nd Population Balance Modeling Webinar
25th November 2024, online

Preparation of w/o/w Double Emulsions in a Stirred Tank: Modeling the Release Kinetics through a Population Balance Framework

Ranim Chakleh[1], Noureddine Lebaz [1] and Nida Sheibat-Othman[1]

[1]LAGEPP/Université de Claude Bernard Lyon1, Villeurbanne, France
Corresponding author: ranim.chakleh@univ-lyon1.fr

ABSTRACT

Double-emulsions (DEs) are liquid-liquid dispersions that consist of one emulsion dispersed within a continuous phase. Common types of DEs include water-in-oil-in-water (w/o/w) and oil-in-water-in-oil (o/w/o) systems. They are typically stabilized by the addition of surfactants at the inner and outer droplets interfaces. DEs can be employed in a wide array of fields including the preparation of reduced-fat food products, pollutant removal in wastewater treatment (i.e. extraction), and encapsulation of active materials in biological and pharmaceutical processes.

In general, DEs are prepared following the two-step method. In the first step a primary emulsion (i.e., internal emulsion), is prepared by dispersing the inner phase into an intermediate phase. This is accomplished under high shear rates using energy-consuming devices such as rotor-stators, high-pressure homogenizers, and ultrasonicators, which generate small droplets. In the second step, the obtained emulsion is dispersed into a continuous phase under lower energy rates. This step can be performed in low energy-consuming devices (e.g., stirred tank, rotor-stator) to avoid extracting the inner emulsion.

Our study focuses on the preparation of w/o/w double emulsions for encapsulation purposes. First, a w/o primary emulsion (water in silicone oil) is prepared using an Ultraturrax (rotor-stator device) in the presence of a lipophilic surfactant (ABIL EM 97S). This emulsion is then dispersed in water in a 1 L stirred tank equipped with a Rushton-type impeller, where the macro (outer) drops are stabilized by a hydrophilic surfactant (Tween® 20) (at the interface between the w/o emulsion drops and external water). Sodium Chloride (NaCl) salt is used as a model encapsulated material dissolved in the inner water. NaCl here serves two purposes: it acts as a tracer to track the release kinetics of the encapsulated material and a regulator of the osmotic pressure as it counterbalances the Laplace pressure to prevent the collapse or swelling of the DEs. The experiments are carried out under various operating conditions and compositions to investigate their effect on the release. These parameters include the viscosity of the oil phase, the inner water content, the concentration of lipophilic and hydrophilic surfactants, the mixing intensity (N) during the second step of preparation, the inner droplet size, and the holdup. The formation of DEs is monitored using an *in situ* probe camera (SOPAT®) and the temporal evolution of the droplet size distribution (DSD) is obtained by a machine-learning-based algorithm developed by Bana et al. (2024). The rate of release is probed by means of a conductivity meter submerged in the stirred tank. This setup allows the measurement of the continuous phase conductivity (given that oil is non-conductive), which is directly correlated to the amount of salt released during the preparation.

In addition, a model for the release kinetics during the second preparation step is proposed. Release of the inner droplets can occur via two possible routes. First, since the DEs droplets are subjected to agitation, the macro-drops are prone to breakage, after which the micro-droplets may leak at a rate R_{leakage}. Second, the micro-droplets near the surface can escape due to the coalescence of the inner water droplets with the continuous aqueous phase at the oil surface, occurring at a rate R_{escape}. It is important to note that the NaCl solubility in oil is negligible, hence the molecular diffusion of NaCl out of the microdroplet is insignificant.

In a previous study, Khadem and Sheibat-Othman (2019) modeled the release kinetic of double emulsions prepared in the second step using an Ultraturrax for a short time (4-16 min) and concluded that the breakage of macro-drops was the main mechanism behind the release. Accordingly, they suggested a model with $R_{\text{leakage}} \propto R_{\text{breakage}}$. However, our experiments suggest that the release may result from the simultaneous breakage of macro drops and coalescence of micro-droplets with the external water phase. This is due to the lower energy dissipation in the stirred tank and longer preparation period compared to the previous work, where the surface coalescence is not negligible.

Figure 1 represents the temporal evolution of the Sauter mean diameter (d_{32}, left y-axis) and the fraction of salt released (right y-axis). The DE is prepared at $N = 300$ rpm for 2 hrs then kept under light agitation (190 rpm) for a couple more hours. It can be discerned that during the initial stage ($N = 300$ rpm) and because of the important breakage of macro-droplets, d_{32} gradually decreases over nearly 1.3 h (the boundary between the white and green areas), while the amount of released salt increases. This suggests that breakage contributes to the release at this stage. After that point, d_{32} remains constant while the amount of released salt continues to increase, albeit at a lower rate, as indicated by the decrease in the slope of the black dashed line. This suggests that another phenomenon is taking place.

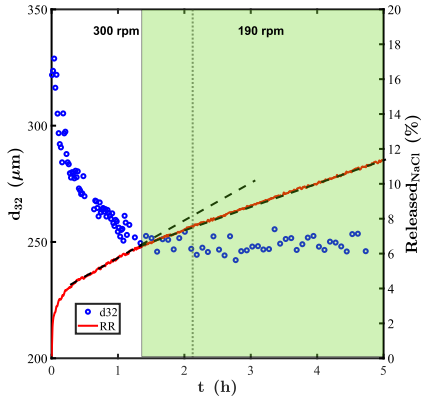

Figure 1. *Temporal evolution of the Sauter mean diameter(d_{32}) of the DE and the % of released salt*

One might think that equilibrium of droplet size is reached after 1.3 h with the breakage of the macro-droplets being counterbalanced by their coalescence, implying that breakage is always behind the release. However, when N was set to 190 rpm -a condition that stops the breakage of macro-drops- d_{32} does not vary which eliminates the possibility of macro-drops coalescence. This is certainly due to the amount of surfactant added and the dilute conditions of preparation (holdup < 3 wt.%). Hence, a possible reason for the further increase in the released salt is the diffusion and coalescence of the inner micro-droplets with the external phase. This phenomenon seems to be more prevalent throughout the preparation step in the stirred tank, compared to the leakage phenomenon. However, both should be included in the release model.

Based on this reasoning, the population balance equation for the volume-based number density function $n(t,v)$ of the macro-drops (cf. Eq. (1)) is coupled to that of micro-droplets (cf. Eq. (2)). In these equations, R stands for rate, Q the volumetric flow rate and v the volume of drops. Finally, the amount of salt released can be calculated based on Eq. (3) where N is the total number of moles of NaCl encapsulated and C is the its concentration.

$$\frac{\partial n_{\text{macro}}(t,v)}{\partial t} + \frac{\partial (Q_{\text{release}}(t,v) n_{\text{macro}}(t,v))}{\partial v} = R_{\text{breakage}} \quad (1)$$

$$\frac{\partial n_{\text{micro}}(t,v)}{\partial t} = -R_{\text{release}}(t,v) = -R_{\text{leakage}}(t,v) - R_{\text{escape}}(t,v) \quad (2)$$

$$\frac{dN}{dt} = -C_{salt} \times Q_{\text{release}} = -\int_0^{\infty} R_{\text{release}}(t,v) v dv \quad (3)$$

Keywords: Double-emulsions, Stirred tank, Encapsulation, Release, Population Balance Modeling.

REFERENCES

Bana, G., Lamadie, F., Charton, S., Randriamanantena, T., Lucor, D., Sheibat-Othman, N., 2024. Front. Chem. Eng. 6, 1415453. https://doi.org/10.3389/fceng.2024.1415453

Khadem, B., Sheibat-Othman, N., 2019. Chem. Eng. J. 366, 587–597. https://doi.org/10.1016/j.cej.2019.02.092

2nd Population Balance Modeling Webinar
25th November 2024, online

Investigating Microorganism Co-Cultures Using Coupled Population Balance Modeling

Fangxing Zhang, Charlotte Deffur and Heiko Briesen

Chair of process systems engineering, Technical University of Munich, Munich, Germany
Corresponding author email: briesen@wzw.tum.de

ABSTRACT

In this study, we apply coupled population balance modeling to investigate fungal-bacterial interactions in a co-cultivation and study how different interactions mechanisms alter the metabolic pathways. Two models are developed to represent distinct mechanisms: one based on the detection of signaling compounds in the solution, and the other via cell-to-cell contact between microorganisms. This work provides us a deeper understanding of microbial behavior and their kinetic mechanisms in the co-cultivation process.

Keywords: coupled population balance model; co-cultivation; microorganism interaction; metabolite pathway activation

1. Introduction

Actinomycetes and filamentous fungi are widely-recognized as a cell factory for producing and secreting proteins, organic acids, and secondary metabolites. Extensive genomic investigations have shown that many of their potential metabolite products remain unexplored. To discover novel metabolites, fungal bacterial co-cultivation is often employed to mimic natural interactions between different species, which can trigger the production of secondary metabolites not observed in monocultures.

The alterations in metabolic pathways during co-cultivation can be distinguished between two primary mechanisms (Deveau et al. 2018):

1. Signal Compounds: One microorganism secretes signal compounds that, upon detection by another, induce changes in its metabolic pathway. This results in the production of novel metabolites not present in monocultures.
2. Cell-to-Cell Contact: During direct interactions between microorganisms, specific outer membrane proteins on the cell membrane influence the physiological responses of neighboring microorganisms.

This study proposes a new expression to describe changes in metabolite pathways resulting from fungal-bacterial interactions during co-cultivation. The influence of various hydrodynamic conditions is studied, which lead to different concentration profile of the novel metabolite.

2. Methods

In the model, fungi and bacteria in submerged culture are represented as porous spherical pellets characterized by their volume. Two conceptually different PBM formulations are used to represent the bacterial-fungal interaction mechanisms (see Table 1). In both mechanisms, the pellets undergo growth, denoted as G. For the signal compounds mechanism, bacteria gradually secrete signaling compounds, and fungi are activated immediately upon detecting these signals. The formation rate of the novel metabolite after pathway activation is modeled using the Luedeking-Piret model (Gomes et al. 2014) and depends on the total fungal biomass. In the cell-to-cell contact mechanism, fungi are categorized as non-activated or activated. Collisions between fungi and bacteria lead to flux exchanges between non-activated and activated fungi, with the collision kernel denoted as f_{A1B}. The formation rate of novel metabolite is primarily driven by the activated fungi.

Table 1. *The PBM formulations for two bacterial-fungal interaction mechanisms.*

Signal Compounds	Cell-to-Cell Contact

Fungi (A): $\frac{\partial N_A(v_A,t)}{\partial t} + \frac{\partial[G_A(v_A)\cdot N_A(v_A,t)]}{\partial v_A} = 0$ Bacteria (B): $\frac{\partial N_B(v_B,t)}{\partial t} + \frac{\partial[G_B(v_B)\cdot N_B(v_B,t)]}{\partial v_B} = 0$ Signaling compound (S): $\frac{\partial c_S}{\partial t} = \alpha_S \cdot \frac{\partial c_S}{\partial t} + \beta_S \cdot c_S$	Fungi before the activation of new metabolite pathway (A1): $\frac{\partial N_{A1}(v_{A1},t)}{\partial t} + \frac{\partial[G_{A1}(v_{A1})\cdot N_{A1}(v_{A1},t)]}{\partial v_{A1}} = -N_{A1}(v_{A1},t) \cdot \int_0^\infty f_{A1B}(v_{A1}, v_B^*) \cdot N_B(v_B^*) dv_B^*$ Fungi after the activation of new metabolite pathway (A2): $\frac{\partial N_{A2}(v_{A2},t)}{\partial t} + \frac{\partial[G_{A2}(v_{A2})\cdot N_{A2}(v_{A2},t)]}{\partial v_{A2}} = +N_{A1}(v_{A2},t) \cdot \int_0^\infty f_{A1B}(v_{A2}, v_B^*) \cdot N_B(v_B^*) dv_B^*$ Bacteria (B): $\frac{\partial N_B(v_B,t)}{\partial t} + \frac{\partial[G_B(v_B)\cdot N_B(v_B,t)]}{\partial v_B} = 0$
Novel metabolite product (X) $\frac{\partial c_X}{\partial t} = (\alpha_X \cdot \frac{\partial c_A}{\partial t} + \beta_X \cdot c_A) \cdot \frac{c_S}{K_{X,i}+c_S}$	Novel metabolite product (X) $\frac{\partial c_X}{\partial t} = \alpha \cdot \frac{\partial c_{A2}}{\partial t} + \beta \cdot c_{A2}$

3. Selected results and Discussion

Using the PBMs described above, we simulated the co-cultivation of microorganisms under different interaction mechanisms and observed parameters that can be experimentally measured. A Cell-to-Cell Contact model with a constant collision kernel was compared with the Signal Compounds model (Figure 1). The biomass-specific concentration of the novel metabolite showed varying trends between the two models. In the Signal Compounds model, where all fungi are activated immediately, the concentration of the novel metabolite increases much more rapidly. In contrast, in the Cell-to-Cell model, only a few fungi are activated initially, leading to a slower concentration rise. However, at later time points, both models exhibit a similar concentration curve, as all fungi eventually become activated.

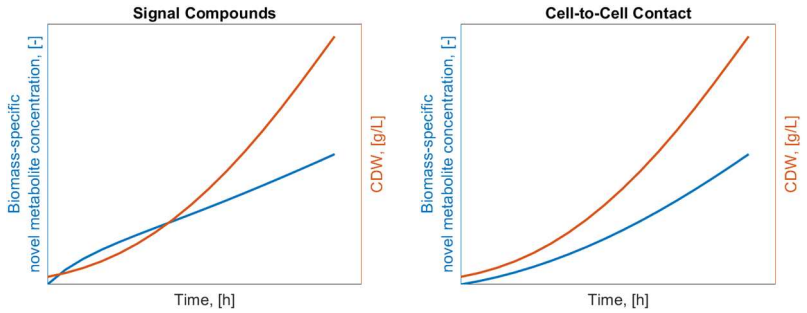

Figure 1. *Simulation results for changes in metabolite pathways: (left) through signal compounds and (right) via cell-to-cell contact. The plots show the biomass-specific concentration of the novel metabolite and the cell dry weight (CDW).*

4. Conclusion

In this study, we introduced new expressions for population balance models to describe changes in microbial metabolic pathways due to interactions with signaling compounds and physical cell-to-cell contact. These new models provide deeper insights into the underlying mechanisms of these interactions, enhancing our understanding of microbial behavior in co-cultivation.

REFERENCES

Deveau, A., 2018. Bacterial–Fungal Interactions: Ecology, Mechanisms and Challenges. *FEMS Microbiology Reviews* 42(3):335–52. doi: 10.1093/femsre/fuy008.

Gomes, J., 2014. Lovastatin Biosynthesis Depends on the Carbon–Nitrogen Proportion: Model Development and Controller Design. *Engineering in Life Sciences* 14(2):201–10. doi: 10.1002/elsc.201300011.

2nd Population Balance Modeling Webinar
25th November 2024, online

Determination of PBE Kernels Using Optimization Methods and PSD Data

Haoran Ji, Frank Rhein

Karlsruhe Institute of Technology, Karlsruhe, Germany
email: haoran.ji@kit.edu

ABSTRACT

This work presents an optimization approach to identify agglomeration and breakage kernels for a discrete population balance equation (dPBE) using particle size distribution (PSD) data. The study focuses on a two-dimensional dPBE with eight kernels requiring optimization. The optimization is performed within a parallelized Ray Tune framework, assessing the impact of different optimization methods and hyperparameters. PSDs generated by the dPBE were used as training targets for model validation. Results demonstrate the efficiency of the optimization framework in accurately determining the kernels.

Keywords: Discrete Population Balance Equation; Agglomeration and Breakage Kernels; Particle Size Distribution; Optimization Framework; Ray Tune.

1. Motivation

The discrete Population Balance Equation (PBE) based on material volume can effectively track the evolution of particle size distribution (PSD) across different components and sizes in various processes, such as material separation and battery slurry preparation. The accuracy of the PBE model's predictions is heavily dependent on the kernels, which are challenging to measure experimentally or calculate analytically with precision.

To address this challenge, this paper proposes an optimization framework based on PSD data to determine the kernels. The framework accepts PSD data from single or binary materials and returns their corresponding kernels. To quantify the error between the optimized kernels and the true values, a dataset generated by the dPBE with various kernel combinations is used for training. This dataset is also employed to test hyperparameters within the optimization framework, offering a comprehensive overview of its performance.

2. Methods

2. 1. Population Balance Equation

In this work, we consider a homogeneous system where both agglomeration and breakage processes occur, leading the PBE to include only agglomeration and breakage terms on its right-hand side. The equation is discretized using the cell average technique of Kumar [1], which allows for the use of a coarse grid to cover systems with a wide range of particle volumes while maintaining computational accuracy. The agglomeration rate and breakage rate are calculated using a Power law model, with collision efficiency modeled by Collision case model (Rhein 2019 [2]). For the breakage function, a Parabolic form in is employed.

2. 2. Optimization Framework

Figure 1 illustrates the general flow of the optimization framework. The primary objective of the optimization framework is to identify a set of kernels such that the PSD calculated by the dPBE using these kernels has the minimal error when compared to the target PSD. The optimization framework supports input from both 1D and 2D PSD data, with a particular emphasis on 2D PSD. A method was implemented that combines 2D-PSD data with the 1D-PSD of each material individually. This integrated approach has proven to significantly improve the optimization outcomes, resulting in more precise kernel determination.

Given that optimizing multiple kernels typically requires numerous iterative steps, improving computational efficiency is essential. To address this, the framework employs Ray Tune [3], which supports parallelized optimization algorithms. Additionally, Ray, as a large-scale distributed computation platform, has the capability to handle the simultaneous optimization of multiple PSD datasets, further enhancing processing efficiency.

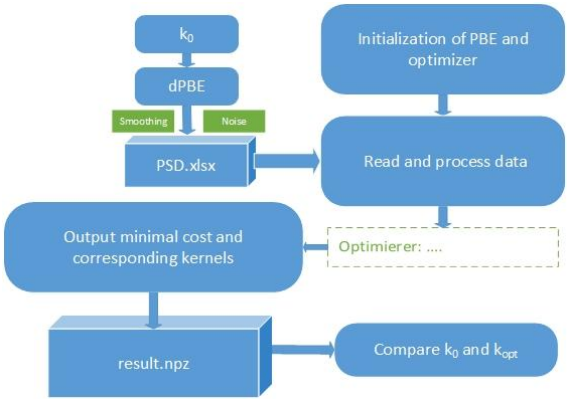

Figure 1. *General process of optimization framework.*

3. Results

The optimization framework was tested against a comprehensive dataset. To ensure the generality of the test, the dataset was generated using reasonable combinations of kernel values. The impact of different optimization algorithms, iteration counts, and optimization criteria on the results was thoroughly evaluated, as shown in Figure 2. Following this, a correlation analysis was conducted to explore the relationship between the error in the optimized kernels and the error in the PSD itself. This correlation analysis provides a foundation for the correct application of the framework and offers insights for further optimizing its functionality.

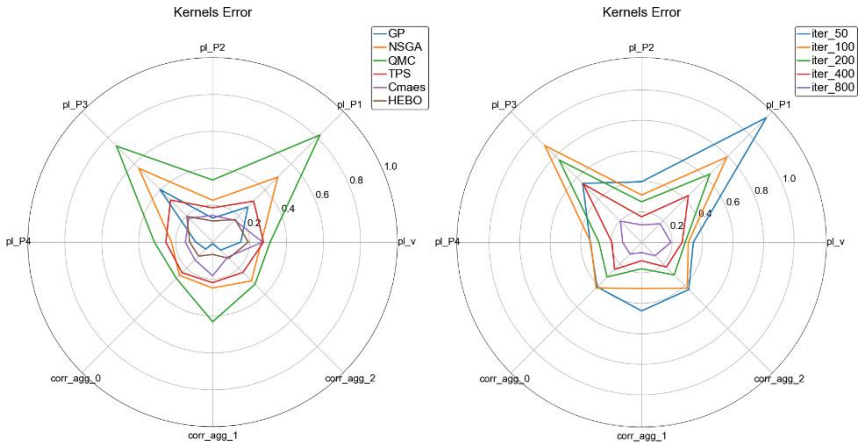

Figure 2. *Impact of the optimization algorithm and the iteration step on the obtained kernels.*

REFERENCES

[1] Kumar, Jitendra. *Numerical approximations of population balance equations in particulate systems*. Diss. Otto-von-Guericke-Universität Magdeburg, Universitätsbibliothek, 2006.

[2] Rhein, Frank, Felix Ruß, and Hermann Nirschl. "Collision case model for population balance equations in agglomerating heterogeneous colloidal systems: Theory and experiment." *Colloids and Surfaces A: Physicochemical and Engineering Aspects* 572 (2019): 67-78.

[3] Liaw, Richard, et al. "Tune: A research platform for distributed model selection and training." *arXiv preprint arXiv:1807.05118* (2018).